ACS APPLIED MATERIALS & INTERFACES

Research Article

www.acsami.org

Self-Assembled Hybrids of Fluorescent Carbon Dots and PAMAM Dendrimers for Epirubicin Delivery and Intracellular Imaging

Ishita Matai,[†] Abhay Sachdev,[†] and P. Gopinath*[,†,‡]

[†]Nanobiotechnology Laboratory, Centre for Nanotechnology, Indian Institute of Technology Roorkee, Roorkee, Uttarakhand-247667, India

[‡]Department of Biotechnology, Indian Institute of Technology Roorkee, Roorkee, Uttarakhand-247667, India

Supporting Information

ABSTRACT: Advanced nanomaterials integrating imaging and therapeutic modalities on a single platform offers a new horizon in current cancer treatment strategies. Recently, carbon dots (CQDs) have been successfully employed for bioimaging of cancer cells. In the present study, luminescent CQDs with anionic terminus and cationic acetylated G5 poly(amido amine) (G5-Ac85) dendrimers were combined via noncovalent interactions to form self-assembled fluorescent hybrids. The fluorescence of CQDs in hybrids is enhanced in the vicinity of primary amine groups of dendrimers, making them suitable as cellular imaging probes. Encapsulation of chemo-drug epirubicin (EPI) in the dendrimer interiors endowed the fluorescent hybrids with therapeutic potential. The *in vitro* release of an entrapped EPI drug from CQDs@EPI⊂G5-Ac85 hybrids was faster in an acidic environment than under physiological conditions. Herein, multifunctional CQDs@EPI⊂G5-Ac85 hybrids serve as a dual-emission delivery system, to track the intracellular distribution and cytotoxic effects of EPI drugs. Green emission properties of CQDs were used for fluorescence microscopic imaging and cellular uptake by flow cytometry. Cell cycle analysis, field-emission scanning electron microscopy (FE-SEM), reactive oxygen species (ROS) generation, and up-regulation of apoptotic signaling genes unanimously demonstrated the apoptosis inducing ability of CQDs@EPI⊂G5-Ac85 hybrids in breast cancer (MCF-7) cells. Therefore, we have evaluated CQDs@EPI⊂G5-Ac85 hybrids as prospective candidates to achieve simultaneous imaging and drug delivery in cancer cells.

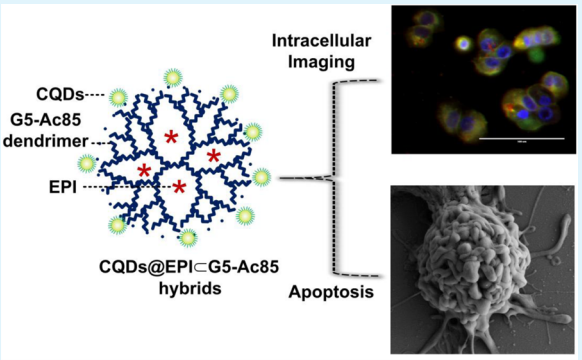

KEYWORDS: *carbon dots, bioimaging, dendrimers, hybrids, epirubicin, drug delivery*

1. INTRODUCTION

With the progress in medical nanotechnology, the demand for multifunctional theranostic nanomaterials to combine the therapeutic and imaging modalities into a single agent has increased.[1] Such advanced nanomaterials are expected to bridge the gap between therapy and imaging for concurrent monitoring of therapy response.[2] Polymer based nanoplatforms such as dendrimers hold great promise for construction of such multifunctional vehicles.[3,4] Well-defined size, three-dimensional architecture, high density of peripheral functional groups, and a multivalent exterior for multiple conjugation reactions makes dendrimers attractive candidates for drug delivery and molecular imaging.[5−7] The unique dendritic architecture resolves the traditional drug delivery problems by enhancing the water solubility and bioavailability of hydrophobic drugs.[8] Among the promising dendritic systems, full generation poly(amido amine) (PAMAM) dendrimers bearing terminal amines have been employed for delivering water-insoluble drugs,[9,10] anticancer agents,[11−14] and oligonucleotides for enhanced gene transfection.[15−18]

Besides delivery, high generation dendrimers have been utilized as a template or stabilizer for metal nanoparticle synthesis.[19] In our previous work, we have demonstrated the use of G5.0 PAMAM dendrimers as stabilizers for forming amine terminated silver nanoparticles (DsAgNPs) and a carrier of anticancer drug 5-fluorouracil (5-FU). Such a multicomponent dendritic system could synergistically induce cell death in breast and lung cancer cells.[20] However, amine terminated PAMAM dendrimers are known to suffer from concentration and generation dependent toxicity. Byrne and coworkers correlated the cytotoxic response of PAMAM dendrimers (G4, G5, and G6) with the generation and hence increasing number of surface amine groups using different *in vitro* and *in vivo* models. The cytotoxicity of PAMAM dendrimers was determined by various biological assays whereby G6 > G5 > G4.[21−24] Hong and group investigated the amine-terminated PAMAM dendrimer interactions with the DMPC (1,2-dimyristoyl-*sn*-glycero-3-phosphocholine) lipid bilayers as well as KB and Rat2 cell membranes. They noted that while high generation G7 PAMAM dendrimers (10−100

Received: March 9, 2015
Accepted: May 6, 2015
Published: May 6, 2015

DOI: 10.1021/acsami.5b02095
ACS Appl. Mater. Interfaces 2015, 7, 11423−11435

nM) caused the formation of nanoscale holes, but G5 PAMAM dendrimers only expanded holes at existing defects.[25] The apparent mechanism behind the nanoholes formation could be removal of lipids by dendrimers or direct insertion of dendrimers into the membrane.[26,27] Thus, the cationic dendritic exterior could be modified to reduce the overall positive charge responsible for its toxicity without compromising its inherent advantages.

Partial surface acetylation or introduction of hydrophilic polymers such as poly(ethylene glycol) (PEG) on the dendrimer periphery can reduce the overall positive charge and hence the cytotoxicity issues of the PAMAM dendrimer.[28−32] Conversion of primary amines to neutral acetamides is considered a relatively simple methodology with regard to complicated surface conjugation reactions.

Epirubicin (4′-epimer of doxorubicin) belongs to the anthracycline family and is widely used for the treatment of breast, stomach, bladder, lung, and ovarian cancers.[33] Epirubicin (EPI) is known to be better tolerated with reduced cardiotoxicity and comparable antitumor efficacy as doxorubicin.[34] However, insufficient EPI delivery (in appropriate concentration) and development of multidrug resistance in cancer cells restrain the achievment of efficient chemotherapy. Incorporation of EPI in polymers such as PAMAM dendrimers can tailor its solubility and hence bioavailability toward cancer cells. The nanosized dendrimer-drug formulations can permeate through the leaky and defective tumor vasculature to accumulate in the tumor region by a well-known enhanced permeability and retention (EPR) effect.[5,18] Tumors with a poor lymphatic drainage system favor selective accumulation of nanoscale drug delivery systems to exhibit maximal therapeutic benefit with minimal side effects.[8] The inherent red fluorescence of EPI is advantageous for cell-internalization studies.

Designing strategies for integrating imaging modalities with dendrimers carrying anticancer drugs for concurrent intracellular tracking and therapy offer a new horizon in cancer treatment. Carbon dots (CQDs) with zero dimension are the newest members in the family of luminescent carbon nanomaterials.[35] They are highly appreciated for their bright fluorescence, high chemical inertness, high solubility, easy functionalization, and low toxicity compared to conventional dyes and toxic semiconductor quantum dots.[36,37] These superior features of carbon dots prompt their use in bioimaging applications.[38−40] Recently, we have synthesized luminescent CQDs through the hydrothermal method and applied them for bioimaging in cancer cells. For this, chitosan was used as the carbonaceous source and poly(ethylene glycol) (PEG) for surface passivation to enhance the fluorescence properties of CQDs. These biocompatible CQDs with bright fluorescence and excellent photostability could label cancer cells with green fluorescence.[39]

Macromolecules such as PAMAM dendrimers with abundant amine terminal groups can form hybrids with other nanomaterials such as low molecular weight CQDs via molecular self-assembly. CQDs with hydroxyl (−OH) surface groups can noncovalently interact with the cationic acetylated PAMAM dendrimers to form fluorescent hybrids. We intentionally adopted a noncovalent pathway for hybrid formation for its several advantages: (i) a relatively simple approach to a variety of hybrid assemblies, (ii) covalent conjugation by surface modification can quench CQD fluorescence, and (iii) enhancement in CQDs fluorescence by PAMAM dendrimer via charge-transfer process.[40,41] Recently, Zhou and co-workers demonstrated use of negatively charged CQDs as caps on positive mesoporous silica nanoparticles (MSPs) for smart delivery of anticancer drug doxorubicin (DOX).[42] Zong and group reported photoluminescence (PL) enhancement of carbon dots in the vicinity of AuNPs conjugated through G4.0 PAMAM NH_2 dendrimers.[43]

In the present study, G5 PAMAM dendrimers with larger interiors than G4 dendrimers (∼5.4 nm) and lower cytotoxicity than G6 dendrimers were selected for hybrid formation. Herein, self-assembled hybrids of CQDs and EPI⊂G5-Ac85 dendrimer complexes (85 refers to peripheral acetyl groups) as CQDs@EPI⊂G5-Ac85 act as a multifunctional dual-emission and therapeutic system. The emission intensity of CQDs is enhanced after noncovalent complexation with EPI⊂G5-Ac85 complexes. To the best of our knowledge, this is the first instance wherein CQDs have been used to visualize and quantitate the intracellular uptake of EPI⊂G5-Ac85 inclusion complexes by fluorescence microscopy and flow cytometry techniques. CQDs@EPI⊂G5-Ac85 hybrids illustrate pH dependent release of encapsulated EPI drugs and serve as imaging probes in the transport process to their target destination. Various cell based assays were performed to investigate the anticancer activity of EPI in encapsulated form in CQDs@EPI⊂G5-Ac85 hybrids in MCF-7 (breast cancer) and NIH 3T3 (mouse embryonic fibroblast) cells. Further, elucidation of the mode of cell death was done by monitoring the cell cycle distribution, ROS levels by flow cytometry, and differential expression of apoptosis related genes by RT-PCR, respectively. Our results indicated that CQDs@EPI⊂G5-Ac85 hybrids could remarkably reduce the MCF-7 proliferation and induce apoptosis by oxidative DNA disintegration and trigger of mitochondrial pathway of apoptosis. The ability of CQDs@EPI⊂G5-Ac85 hybrids for synchronized bioimaging and drug delivery has been confirmed to achieve improved cancer diagnosis and therapy.

2. EXPERIMENTAL SECTION

Materials. Ethylenediamine core amine-terminated G5 PAMAM dendrimers (M_w 28824.81 g mol^{-1}) with a polydispersity index of less than 1.08 was purchased from Sigma-Aldrich, USA. Acetic anhydride and triethylamine were obtained from Thomas Baker, India. Epirubicin hydrochloride (EPI·HCl) was bought from Sigma-Aldrich, USA. Chitosan and poly(ethylene glycol) (PEG) were purchased from SRL, India. Glacial acetic acid was obtained from SDFCL, India. A regenerated cellulose dialysis membrane (molecular weight cut off, MWCO = 10 kDa) was acquired from Thermo Fisher Scientific, USA. 3-(4,5-Dimethyl-2-thiazoyl)-2,5-diphenyltetrazolium bromide) (MTT), 2′,7′-dichlorofluorescin diacetate (DCFDA), and 3,8-diamino-5-[3-(diethylmethylammonio)propyl]-6-phenylphenanthridinium diiodide (PI) were obtained from Sigma-Aldrich, USA. Dulbecco's minimum essential medium (DMEM) and phosphate buffer saline (DPBS; Ca^{2+} and Mg^{2+} free) powders purchased from Sigma-Aldrich, USA were reconstituted prior to use. For all the preparations, ultrapure water (18 MΩ cm) was used.

Surface Acetylation of G5 PAMAM Dendrimers. The ratio between acetic anhydride and the dendrimer was adjusted to convert 70% primary amines on the surface to acetamide groups. The stoichiometric ratio of primary amines/acetic anhydride was kept at 1:1 to achieve the desired extent of surface acetylation.[31] The typical procedure adopted for the synthesis of partially acetylated PAMAM dendrimers is as follows. G5 PAMAM (31.7 mg, 1.1×10^{-3} mmol) in 10 mL of dry methanol was allowed to react with acetic anhydride (9.4×10^{-3} mL, 9.9×10^{-2} mmol) in the presence of triethylamine (10% molar excess of acetic anhydride) under stirring conditions at room

DOI: 10.1021/acsami.5b02095
ACS Appl. Mater. Interfaces 2015, 7, 11423−11435

temperature. Triethylamine was added to quench acetic acid, a side product formed in the reaction. The solution was stirred for 24 h under an argon atmosphere, and methanol was removed under a vacuum to obtain a white colored polymer residue. The polymer residue was redissolved in water and dialyzed against 1 L of PBS followed by water for 3 days using a dialysis membrane (MWCO = 10 kDa). The purified samples were then lyophilized and stored at −20 °C. The number of primary amines acetylated was determined by ^{1}H NMR analysis and was found to be 85 groups.

Encapsulation of EPI within G5-Ac85 Interiors. G5-Ac85 dendrimers (10 mg, 0.3 × 10^{-3} mmol) were dissolved in 1.5 mL of water. Separately, EPI·HCl with 10 mol equiv of dendrimers was dissolved in 300 μL of methanol and neutralized with 5 μL of triethylamine to generate a water-insoluble EPI solution. The EPI solution was then slowly added to the 1.5 mL of dendrimer aqueous solution and magnetically stirred overnight to allow evaporation of methanol solvent. The EPI⊂G5-Ac85 mixture solution was then centrifuged at 7000 rpm for 10 min to remove the precipitates related to noncomplexed free EPI. The supernatants were analyzed spectrophotometrically at 481 nm using an ultraviolet−visible (UV−vis) spectrometer for indirect determination of EPI encapsulation efficiency. The encapsulation efficiency (EE, %) was calculated as follows:

$$\text{EE (\%)} = \frac{\text{Weight of EPI in G5−Ac(85) dendrimers}}{\text{Weight of EPI fed initially}} \times 100$$

Different concentrations of EPI were used to make the EPI calibration curve. For the data fitting, the least-squares approach was used (the regression equation and correlation coefficient at 481 nm were $y = 0.0135x - 0.0465$ and 0.9985, respectively). The supernatant was lyophilized for 3 days to obtain EPI⊂G5-Ac85 inclusion complexes and kept at −20 °C for further study.

Synthesis of Hydroxyl-Functionalized Carbon Dots (CQDs). Fluorescent CQDs were synthesized as previously reported by our team.[39] Chitosan was used as the carbonaceous source and PEG-4000 as the passivating agent. Briefly, 400 mg of chitosan was dissolved in 60 mL of water under stirring conditions, followed by the addition of 300 μL of acetic acid to obtain a homogeneous solution. To this, 400 mg of PEG-4000 powder was added and stirred until dissolved. The homogeneous solution was then shifted to the hydrothermal reactor and sealed. The mixture was then heated at 200 °C for 8 h under a N_2 atmosphere. Upon cooling, the solution was centrifuged at 9000 rpm for 20 min to separate the insoluble precipitates from the pure CQDs.

Preparation of CQDs@EPI⊂G5-Ac85 Fluorescent Hybrids. The CQDs@EPI⊂G5-Ac85 hybrids were prepared by conjugating hydroxyl terminated CQDs with cationic EPI⊂G5-Ac85 dendrimer complexes. Typically, 50 μL of 1.33 mg mL^{-1} aqueous CQD stock solution was incubated with EPI⊂G5-Ac85 dendrimers with varying concentrations of EPI (0.625, 1.25, 2.5, 5, and 10 μM) under shaking conditions. Finally, the mixture solution was diluted with 250 μL of ultrapure water and left to react for 24 h at room temperature to obtain CQDs@EPI⊂G5-Ac85 fluorescent hybrids. The amount of CQDs in the hybrids was kept fixed, and its final concentration was 0.221 mg mL^{-1}.

***In Vitro* Release of EPI from CQDs@EPI⊂G5-Ac85 Hybrids.** The release of EPI from hybrids was studied under different pH conditions using an acetate buffer (20 mM, pH 5.5) and PBS (20 mM, pH 7.4) at the same time intervals. A total of 2 mL of CQDs@EPI⊂G5-Ac85 hybrid solution was placed equally in two dialysis bags (MWCO 3500 Da), and the receptor compartments were filled with 10 mL of acetate or PBS buffer with mild agitation (70 rpm). After each interval, that is 1, 2, 3, 4, 5, 6, 8, 10, 12, 24, and 48 h, 5 μL of each buffer solution was withdrawn and measured for EPI absorbance by microvolume spectrophotometer. The concentration of EPI was estimated from the dose-absorption curve of EPI. The percentage of EPI released was quantitated as follows:

$$\text{EPI release (\%)} = \frac{\text{EPI released in medium}}{\text{EPI loaded in CD-G5-Ac(85) hybrids}} \times 100$$

Characterization. *UV−Visible Spectroscopic Measurements.* Absorption measurements were performed using a Lasany LI-2800, UV−vis spectrophotometer.

Fluorescence Measurements. Fluorescence spectra were recorded using a Hitachi F-4600 fluorescence spectrophotometer. Fluorescence lifetime measurements were acquired with a Fluoro Cube Fluorescence Lifetime System (Horiba Jobin Yvon) equipped with a Nano LED (635 nm) source. The decay curves were analyzed with IBH decay analysis v 6.1 software.

Zeta and Dynamic Light Scattering (DLS) Measurements. The zeta potential and hydrodynamic diameter of CQDs@EPI⊂G5-Ac85 hybrids were estimated using Malvern Nano ZS 90, Zetasizer operating at 25 °C.

Transmission Electron Microscopy (TEM). The morphology of CQDs@EPI⊂G5-Ac85 fluorescent hybrids was determined by FEI TECHNAI G2 TEM at an operating voltage 200 kV. A total of 10 μL of CQDs@EPI⊂G5-Ac85 hybrids was drop casted onto a carbon coated copper grid and was viewed after negative staining with 2% phosphotungstic acid (PTA).

Nuclear Magnetic Resonance (^{1}H NMR) Measurements. Samples were dissolved in millimolar concentrations in D_2O solvent, and ^{1}H NMR spectra were acquired using a Bruker 500 MHz NMR spectrometer.

Cell Culture. MCF-7 (human breast adenocarcinoma) and NIH 3T3 (mouse embryonic fibroblast) cells were obtained from the National Centre for Cell Sciences (NCCS) Pune, India and cultured in a DMEM medium containing 10% (v/v) fetal bovine serum (FBS, Gibco Life Technologies) and 1% (v/v) penicillin−streptomycin (Sigma-Aldrich, USA) and kept at 37 °C in a 5% CO_2 incubator. When the cultured cells reached 70−80% confluence, harvesting was done using 0.25% trypsin-EDTA.

Cytotoxicity Assay. An MTT assay was used to determine the cellular viability. Cells were seeded in a 96-well assay plate at a density of 10 000 cells/well (100 μL total volume/well) for 24 h. Free EPI, EPI⊂G5-Ac85 complexes and CQDs@EPI⊂G5-Ac85 hybrids (with equivalent EPI concentrations) were then added to fresh cell culture medium for 48 h of incubation at 37 °C. Free CQDs and G5-Ac85 dendrimers with equivalent mass concentration as in CQDs@EPI⊂G5-Ac85 hybrids were used as controls. Following treatment, a PBS wash was given to remove residual particles. Live cells with active mitochondria can convert the tetrazolium salt to purple formazon crystals. A total of 10 μL of MTT dye was added per well of the assay plate and left for 3 h in 5% CO_2 at 37 °C for the appearance of formazon. After 3 h, the medium was aspirated from each well, and 100 μL of DMSO was added to dissolve the formazon product. The absorbance of purple formazon product at 570 nm was quantitated using a microplate reader (Cytation3, Biotek). All of the experiments were performed in triplicate. Cell viability (%) was expressed as

$$\text{Cell Viability (\%)} = \frac{\text{(A570-A690) treated cells}}{\text{(A570-A690) control cells}} \times 100$$

Intracellular Colocalization Imaging. For cellular imaging, MCF-7 cells (1 × 10^5 cells/mL) were seeded in 35 mm culture dishes and cultured overnight. Following attachment, free CQDs, free EPI, EPI⊂G5-Ac85, and CQDs@EPI⊂G5-Ac85 hybrids with final EPI concentrations (5 μM) were added to a fresh DMEM medium and left for 12 h of incubation at 37 °C. After treatment, cells were washed with PBS twice, and the nucleus was stained with 2 μL of Hoechst 33342 dye (10 mg mL^{-1}) for 10 min. Cells were then analyzed for fluorescent signals using inverted fluorescent microscopy (EVOS FL Color, AMEFC 4300). For imaging, the filters used were DAPI (λ_{ex} 360 nm, λ_{em} 447 nm), GFP (λ_{ex} 470 nm, λ_{em} 525 nm), and RFP (λ_{ex} 530 nm, λ_{em} 593 nm).

Cellular Uptake Studies. Quantitative estimation of cellular uptake of CQDs@EPI⊂G5-Ac85 hybrids was done using a flow cytometer. CQDs exhibit bright green fluorescence with a 488 nm excitation laser in Ch. 02 (505−560 nm), and this enables tracking distribution of hybrids inside the cells. MCF-7 cells (2 × 10^5 cells/mL) were plated in 35 mm culture dishes and cultured overnight. Subsequently, the

DOI: 10.1021/acsami.5b02095
ACS Appl. Mater. Interfaces 2015, 7, 11423−11435

Scheme 1. Schematic Representation of (A) Synthesis of Partially Acetylated G5 PAMAM Dendrimers (G5-Ac85), (B) Encapsulation of Anticancer Drug Epirubicin (EPI) in the Cavities of G5-Ac85 Dendrimers, (C) Synthesis of CQDs@EPI⊂G5-Ac85 Hybrids via Noncovalent Interactions

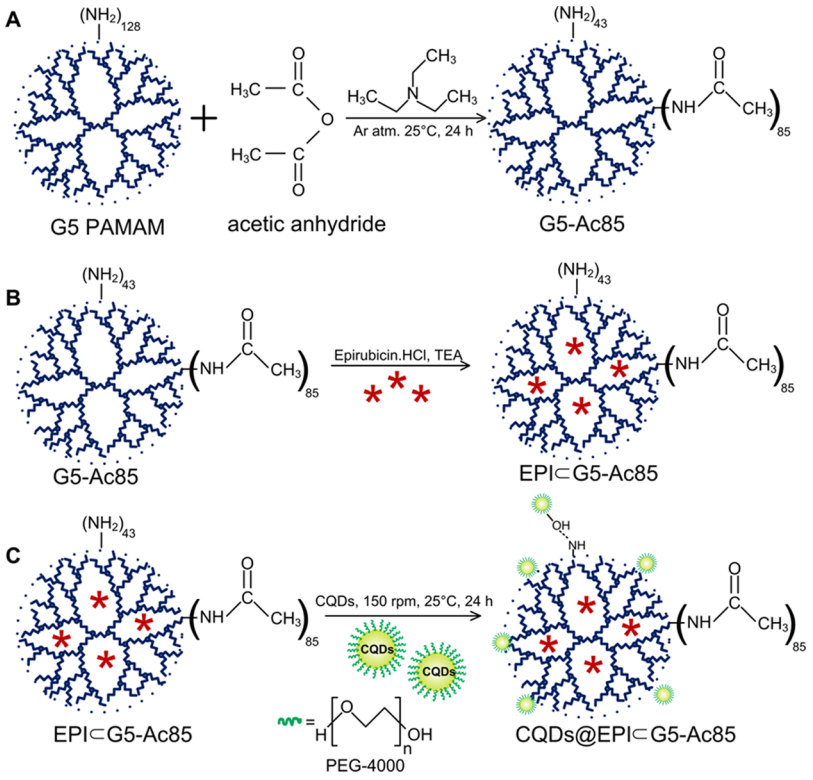

medium was removed and fresh DMEM medium containing CQDs, EPI⊂G5-Ac85, and CQDs@EPI⊂G5-Ac85 hybrids were added to cells. After 3 h of incubation, cells were washed, trypsinized, and centrifuged at 600*g* for 6 min. The cell pellet obtained was redispersed in 200 μL of PBS and analyzed by flow cytometer (Amnis Flowsight). A total of 10 000 events were recorded per sample and analyzed by Amnis Ideas software.

Cell Cycle Analysis. Induction of apoptotic mode of cell death was determined by propidium iodide (PI) staining and subsequent analysis by flow cytometry. MCF-7 cells at a density of 2×10^5 cells/mL were seeded in 35 mm culture plates for overnight attachment. Free CQDs, Free EPI, EPI⊂G5-Ac85, and CQDs@EPI⊂G5-Ac85 hybrids (with final dose of EPI 5 μM) were then added to fresh cell culture medium. After 48 h of incubation, the medium was carefully removed to prevent a loss of floating cells, washed with PBS, trypsinized, and harvested by centrifugation at 200*g* for 5 min. Cells were then fixed with 70% alcohol in ice for 15 min. Next, fixed cells were stained with PI staining solution (50 μg/mL PI, 1 mg/mL RNase A, and 0.05% triton X-100) for 45 min at 37 °C in dark. The amount of PI-labeled DNA was then measured from the cell cycle distribution using a flow cytometer (Amnis Flowsight). A total of 10 000 cells was analyzed for fluorescent signals per sample.

Cell Morphology Analysis by FE-SEM. MCF-7 cells were seeded on sterile glass coverslips in 35 mm culture plates and nursed for 24 h. After that, CQDs@EPI⊂G5-Ac85 hybrids were added to the cells and kept for 24 h. Cells without hybrids were cultured in media and used as a control sample. After treatment, the cells were washed with PBS and fixed in 2% glutaraldehyde solution for 10 min followed by ethanol gradient fixation (20%, 40%, 60%, and 80%). The air-dried samples were then gold sputtered and examined by FE-SEM (QUANTA 200-FEG) operating at 10 kV.

Generation of Intracellular Reactive Oxygen Species (ROS). ROS production in MCF-7 and NIH 3T3 cells when exposed to CQDs@EPI⊂G5-Ac85 hybrids was determined by DCFH-DA staining. DCFH-DA is a nonfluorescent dye which can permeate through the plasma membrane into the cells' interior where it is hydrolyzed to DCFH. In the presence of intracellular ROS, DCFH is oxidized to green fluorescent DCF, which can be quantified. For this assay, cells (2×10^5 cells/mL) were seeded in six-well culture dishes and were grown overnight. Thereafter, cells were exposed to varied concentrations of CQDs@EPI⊂G5-Ac85 hybrids for 12 h, harvested, and washed with PBS. The cell pellet was then redispersed in PBS with 20 μM DCFH-DA and incubated for 10 min at 37 °C in the dark. Immediately after incubation, cells were analyzed for DCF fluorescence using a flow cytometer (Amnis Flowsight). A total of 10 000 events were acquired per sample, and ROS generation was estimated in terms of percentage of cells with DCF (green) fluorescence using Amnis Ideas software.

Semiquantitative RT-PCR Analysis. For gene expression studies, MCF-7 cells were plated in 35 mm culture plates and subsequently treated with Free CQDs, EPI⊂G5-Ac85, and CQDs@EPI⊂G5-Ac85 hybrids (final EPI concentration was 5 μM) for 48 h. Differential expression of apoptotic signaling genes was determined by reverse transcriptase-polymerase chain reaction (RT-PCR). The housekeeping β-actin gene was used as an internal control. Total RNA was isolated from cells using Trireagent (Sigma-Aldrich, USA). After that, cDNA was generated from total denatured RNA (1 μg) by reverse transcription performed at 42 °C for 50 min using Super Script II Reverse Transcriptase (Life Technologies, India) in a total mixture of 20 μL. The steps include an initial denaturation (94 °C for 3 min) followed by PCR cycle of denaturation (94 °C for 30 s), annealing (60 °C for 30 s), extension (72 °C for 1 min), and a final extension (72 °C for 10 min). Finally, the PCR products were resolved on a 1.2% agarose gel and visualized by ethidium bromide staining under UV light. The fold difference was calculated using Image lab 4.0 software in the same instrument.

Statistical Analysis. The values are expressed as mean ± standard error mean (SEM) for all experiments. The data were analyzed via Student's *t* test or via two-way ANOVA, whichever was applicable, using GraphPad Prism 6.0, and statistically significant values are denoted by *($p < 0.05$), **($p < 0.005$), and ***($p < 0.001$).

DOI: 10.1021/acsami.5b02095
ACS Appl. Mater. Interfaces 2015, 7, 11423−11435

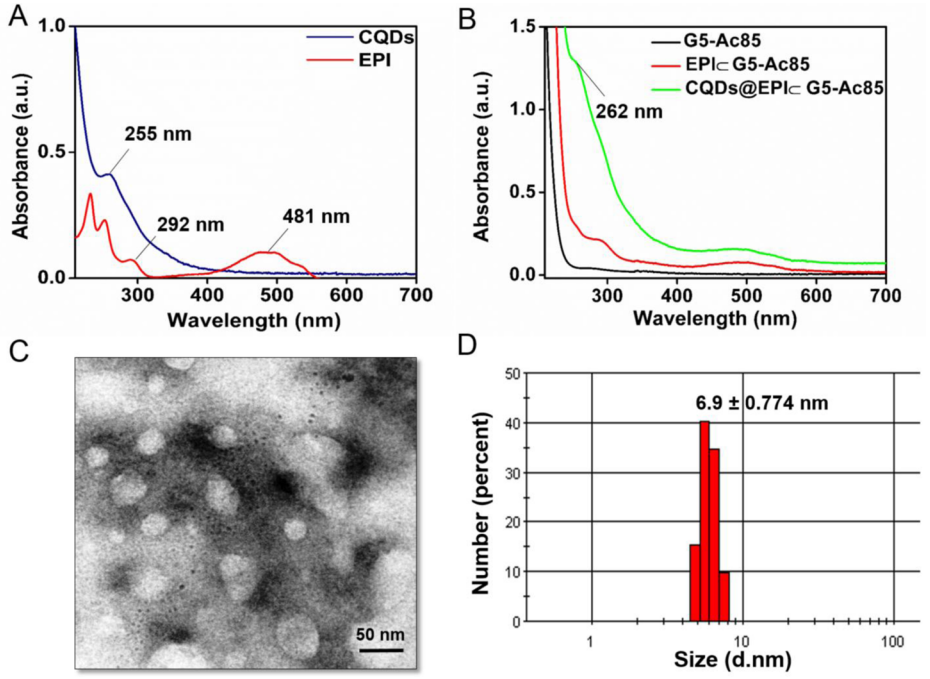

Figure 1. UV−visible spectrum of (A) CQDs in water and EPI in methanol. (B) Aqueous solution of G5-Ac85, EPI⊂G5-Ac85 complexes, and CQDs@EPI⊂G5-Ac85 hybrids. (C) TEM image of as-synthesized CQDs@EPI⊂G5-Ac85 hybrids (with 50 nm scale bar) and (D) size distribution profile by DLS measurements at pH 7.0.

3. RESULTS AND DISCUSSION

Theoretically, the G5 PAMAM dendrimer has 128 primary amine groups on its surface available for modification or functionalization. The chemistry of these terminal groups render a dendrimer with unique properties of water-solubility and reactivity. Exploiting the potential of PAMAM dendrimers as delivery systems while reducing its cytotoxicity is highly appreciable. With this perspective, a fraction of primary amines were converted to neutral acetamide groups, to reduce its toxicity. In this study, the stoichiometric ratio of acetic anhydride/amine groups was kept at 90:1 to achieve 70% conversion of surface amines to acetamides. The ^{1}H NMR spectra of the acetyl-derivatized G5 PAMAM shows a peak at 1.9 ppm corresponding to $-CH_3$ protons of the acetyl group (Figure S1). The peaks at 2.2−3.4 ppm can be assigned to the $-CH_2-$protons of G5 PAMAM.[20,31] The number of acetylated primary amines was determined by comparing the intensity of the $-CH_3$ protons of the acetyl groups to the sum of all $-CH_2$ peaks. From NMR integration, the $-CH_3/-CH_2-$ ratio was calculated, and 85 primary amine groups were functionalized to acetamides to yield G5-Ac85 dendrimers. The obtained partially acetylated molecules are expected to be more compact and water-soluble, compared to pristine dendrimers due to minimal charge-repulsion from reactive primary amines.[31]

Next, EPI·HCl was neutralized with triethylamine to form water-insoluble EPI to enable its efficient encapsulation within G5-Ac85 hydrophobic interiors. This new formulation of EPI⊂G5-Ac85 complexes is expected to enhance the water solubility and thus bioavailability of EPI. This drug-dendrimer formulation was stored in −20 °C and was stable for 1−2 months without any loss in EPI activity. Additionally, hydroxyl (−OH) functionalized carbon dots (CQDs) were synthesized hydrothermally using chitosan as a carbon source and PEG-4000 polymer as the passivating agent. Use of a suitable passivating agent is known to enhance the fluorescence properties of CQDs.[39] CQDs with −OH overhangs can form hybrids with cationic EPI⊂G5-Ac85 nanocomplexes through noncovalent linkages such as hydrogen-bonding and electrostatic interactions to track the intracellular distribution of EPI. Step-wise representation of synthesis of CQDs@EPI⊂G5-Ac85 hybrids is shown in Scheme 1. Such EPI loaded CQDs@G5-Ac85 hybrids are expected to act as multifunctional dual-emission delivery systems.

The formed CQDs@EPI⊂G5-Ac85 hybrids were characterized by UV−vis spectroscopy. The absorption spectra of aqueous CQDs solution and EPI dissolved in methanol were also recorded for comparison. CQDs display a single absorption band at 255 nm, which can be attributed to $\pi-\pi^*$ transition of the conjugated C═C band[39,44] (Figure 1A). EPI exhibits a characteristic band at 481 nm (Figure 1A). Upon EPI encapsulation, G5-Ac85 complexes exhibit an absorption enhancement at a 481 nm peak when compared to blank G5-Ac85 dendrimers (Figure 1B). This suggests complete entrapment of EPI within the G5-Ac85 interiors. The amount of EPI payload in G5-Ac85 dendrimers was determined from the dose-absorption curve of EPI, and encapsulation efficiency was calculated as 57.36 ± 1.5%. With the formation of CQDs@EPI⊂G5-Ac85 hybrids, the absorption band of CQDs was slightly red-shifted to 262 nm, suggesting interaction between the terminal amines and −OH groups of CQDs.

Additionally, the zeta potential (ζ) measurements were also recorded to study the surface charge and interactions among various components of nanocomplexes. The zeta potential of CQDs and G5-Ac85 dendrimers was −18.5 and +16 mV, respectively. After EPI encapsulation, the zeta of G5-Ac85 dendrimers reduced to +11.6 mV, indicating its entrapment within the dendritic architecture. The interactions between the −COOH groups of EPI and interior tertiary amines of G5-Ac85 dendrimers can be held responsible for the formation of EPI⊂G5-Ac85 complexes. After adding CQDs, the zeta

DOI: 10.1021/acsami.5b02095
ACS Appl. Mater. Interfaces 2015, 7, 11423−11435

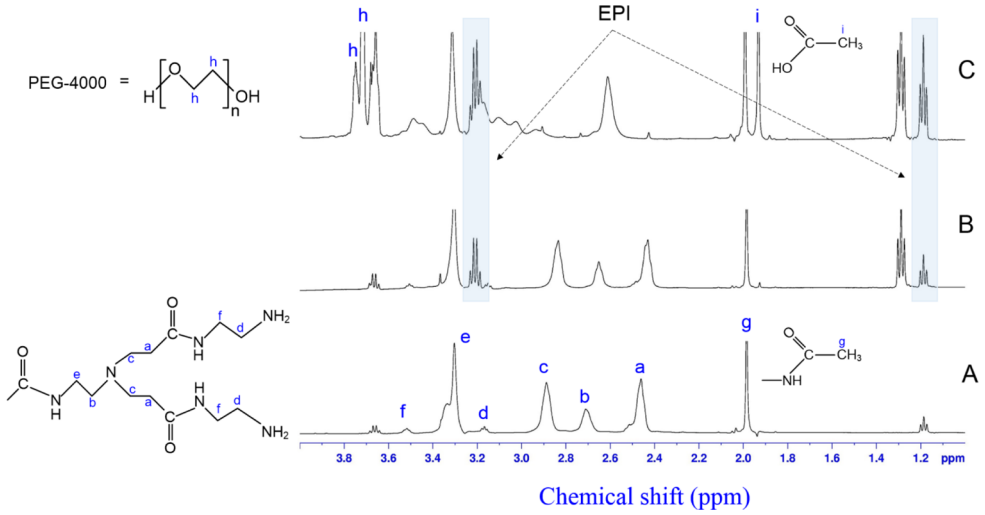

Figure 2. ^{1}H NMR spectra of (A) G5-Ac85, (B) EPI⊂G5-Ac85 complexes, and (C) CQDs@EPI⊂G5-Ac85 hybrids in D_2O. The highlighted portions (blue) represent the characteristic peaks of EPI.

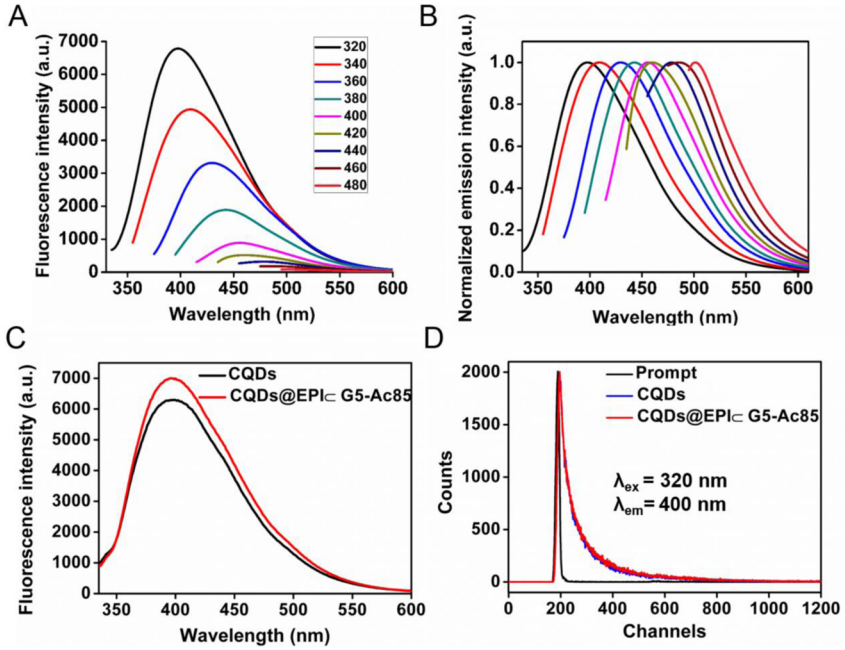

Figure 3. (A) Fluorescence emission spectra of CQDs in water at different excitation wavelengths. (B) Normalized emission spectra. (C) Comparative emission spectra and (D) fluorescence decay profile of CQDs and CQDs@EPI⊂G5-Ac85 hybrids, respectively (λ_{ex} = 320 nm; λ_{em} = 400 nm).

potential further reduced to +8.74 mV, which indicates efficient grafting of anionic CQDs on the cationic EPI⊂G5-Ac85 surface. The overall positive charge of hybrids makes them suitable candidates for bioapplications such as cellular imaging and for drug delivery.[44,45]

Further, TEM investigation was done to predict the morphology and size of CQDs and CQDs@EPI⊂G5-Ac85 hybrids. The as-synthesized CQDs appeared nearly spherical with an average size of 1.75 ± 0.474 nm (Figure S2). Negative staining with PTA revealed uniform EPI⊂G5-Ac85 complexes uniformly decorated with CQDs (black spots) to form CQDs@EPI⊂G5-Ac85 hybrids (Figure 1C). DLS measurements showed that the hydrodynamic diameter of as-prepared hybrids was 6.9 ± 0.774 nm (Figure 1D). It is important to mention that DLS predicts the complete hydrodynamic size of particles.[46]

The formation of EPI⊂G5-Ac85 complexes and CQDs@EPI⊂G5-Ac85 hybrids was further confirmed by ^{1}H NMR measurements using D_2O as a solvent (Figure 2). TSP (3-(trimethylsilyl) propionic-2,2,3,3,-d_4 acid, sodium salt) was used as an internal standard. From Figure 2C, the peak at 1.99 ppm can be assigned to methyl protons of acetamides and peaks at 2.46, 2.71, 2.9, 3.17, 3.32, and 3.52 ppm are representative of the structural protons in an acetylated dendrimer.[47] With EPI encapsulation (Figure 2B), characteristic peaks of methyl protons of EPI at 1.3 and 3.2 ppm were observed along with acetylated dendrimer proton peaks.[48] Moreover, for the structural peaks assigned at "b" and "c" positions, a slight upfield shift from 2.71 to 2.65 ppm and 2.9 to

DOI: 10.1021/acsami.5b02095
ACS Appl. Mater. Interfaces 2015, 7, 11423−11435

2.8 ppm appeared after EPI complexation, reflecting interaction of EPI molecules with dendrimer secondary amines. The other peaks retained their original positions. With the formation of CQDs@EPI⊂G5-Ac85 hybrids, peaks at ∼3.7 and 1.93 ppm were seen in conjunction with the other peaks (Figure 2A). These can be attributed to methylene protons of the PEG moiety and remnant acetic acid in CQDs.[49] The presence of representative NMR peaks of EPI and CQDs indicates the successful formation of EPI⊂G5-Ac85 complexes and CQDs@EPI⊂G5-Ac85 hybrids.

The aqueous solution of CQDs displays the molecular signature excitation dependent emission behavior[39] (Figure 3A). Incrementing excitation wavelength from 320 to 480 nm resulted in a progressive red shift in its maximum emission from 400 to 490 nm, with a reduction in emission intensity. The maximum emission of CQDs was recorded at an excitation wavelength of 320 nm. It is worth mentioning that CQDs at 480 nm excitation have negligible emission, resulting in minimal interference with the EPI emission signal. Interestingly, an enhancement in fluorescence of CQDs in CQDs@EPI⊂G5-Ac85 hybrids was encountered compared to blank CQDs (Figure 3C). This can be ascribed to the electron charge transfer from G5-Ac85 dendrimers to CQDs.[43,50] To confirm this, the fluorescence lifetime decay curves for CQDs and CQDs@EPI⊂G5-Ac85 hybrids were recorded. The obtained data could be fitted to a triple-exponential decay curve, and their average lifetimes were calculated (Figure 3D and Table S1). The average fluorescence lifetime of bare CQDs was 5.84 ns, which increased to 6.12 ns in CQDs@EPI⊂G5-Ac85 hybrids. Thus, grafting of negatively charged CQDs on the PAMAM surface could be a simple and effective strategy for fluorescence enhancement of CQDs.

The effect of change in pH on fluorescence properties of CQDs and CQDs@EPI⊂G5-Ac85 hybrids was also investigated. The emission intensity of both bare CQDs and CQDs@EPI⊂G5-Ac85 hybrids varied with a change in pH of the medium (Figure S3). The fluorescence intensity of CQDs increased steadily in the pH range of 4.0−10.0. However, a slight red shift in emission was monitored from pH 7.0 onward (Figure S3A). With an increase in pH, the terminal −OH groups of CQDs get ionized which influence electronic transitions resulting in such pH dependent behavior. Contrarily, for CQDs@EPI⊂G5-Ac85 hybrids, maximum fluorescence was evident in an acidic environment (pH 5.5) followed by neutral and alkaline conditions (pH 7.0−10.0; Figure S3B). This can be attributed to the protonation of surface amino groups of PAMAM under acidic conditions and deprotonation under alkaline conditions.[39,51,52] Their colloidal stability of bare CQDs and CQDs@EPI⊂G5-Ac85 hybrids was also affected with variation in pH (Figure S4). The zeta potential of CQDs was at a maximum of −21.64 mV at pH 10.0 but reduced to −18.5 mV at pH 7.0 and became low under acidic conditions. Conversely, CQDs@EPI⊂G5-Ac85 hybrids were found to exhibit maximum stability at pH 5.5 with a zeta potential of +28.9 mV. The pH dependent stability estimations of CQDs and CQDs@EPI⊂G5-Ac85 hybrids are in agreement with the fluorescence results.

Another important parameter is the ability of CQDs@EPI⊂G5-Ac85 hybrids to release the EPI payload in a sustained manner. Before evaluating the anticancer activity, the pH controlled release of EPI by CQDs@EPI⊂G5-Ac85 hybrids was investigated *in vitro* at pH 5.5 and 7.4, respectively. The time-dependent release profiles of EPI are shown in Figure 4.

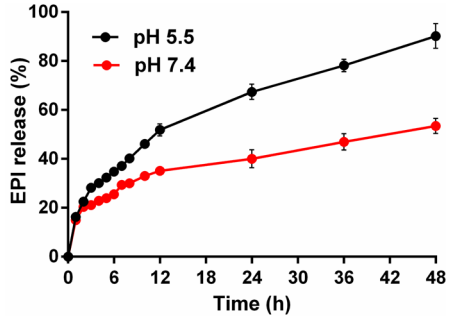

Figure 4. Time-dependent *in vitro* release profiles of EPI (in %) from CQDs@EPI⊂G5-Ac85 hybrids over 48 h in an acetate buffer (pH 5.5, black) and in phosphate buffered saline (pH 7.4, red), respectively.

These hybrids were able to release EPI in a biphasic pattern, characterized by an initial rapid release followed by sustained release. About 90% of EPI was released after 48 h at pH 5.5, imitating the tumor microenvironment. However, around 51% was released in the same time at pH 7.4, close to physiological conditions. The rapid EPI release under acid conditions may be due to weakened electrostatic interactions between protonated interior amines and −CONH− linkages of CQDs@G5-Ac85 hybrids with −COOH groups of EPI molecules.[51] The slow release of EPI from CQDs@G5-Ac85 hybrids at physiological pH compared to that under an acidic environment makes it a suitable candidate for specifically targeting the cancerous cells.

We further investigated the anticancer effects of released EPI from EPI⊂G5-Ac85 complexes and CQDs@EPI⊂G5-Ac85 hybrids *in vitro*. As shown in Figure 5A, MCF-7 cells treated with blank G5-Ac85 dendrimers exhibited a good cell viability at all tested concentrations. This suggests that the introduction of a small acetyl moiety on the dendrimer peripheral surface could improve its cytocompatibility. Free CQDs were also able to maintain appreciable cell viability. Free EPI was found to significantly inhibit the cell growth at all studied doses. With an increase in EPI concentration from 0.625 to 10 μM, the cell viability reduced to nearly 16%. Importantly, CQDs@EPI⊂G5-Ac85 hybrids and EPI⊂G5-Ac85 complexes were also able to inhibit cancer cell proliferation significantly. For instance, at an EPI concentration of 5 μM, around 85% of cells died with free EPI and almost 70% cells died with CQDs@EPI⊂G5-Ac85 and EPI⊂G5-Ac85 treatments. Since G5-Ac85 dendrimers did not alter the cell survival, the toxicity was solely induced by the loaded EPI drug. Also, the addition of CQDs to EPI⊂G5-Ac85 complexes did not affect significantly the exhibited toxic response. We also examined the effect of CQDs@EPI⊂G5-Ac85 hybrids on normal NIH 3T3 cells. At a similar dosage, the hybrids exhibited more inhibitory effect on MCF-7 cells compared to normal cells (Figure 5B). Based on the therapeutic profile of EPI⊂G5-Ac85 complexes and CQDs@EPI⊂G5-Ac85 hybrids, 5 μM EPI concentration was selected for further cell-based experiments.

Next, CQDs were examined as fluorescent probes to monitor the intracellular trafficking of CQDs@EPI⊂G5-Ac85 hybrids in MCF-7 cells. Fluorescence microscope imaging is a promising technique to discern the cellular uptake of fluorescent nanomaterials. Figure 6 shows the fluorescence microscopic images of MCF-7 cells incubated with CQDs, EPI, EPI⊂G5-Ac85 complexes, and CQDs@EPI⊂G5-Ac85 hybrids under similar conditions. CQDs appeared intensely green under blue illumination (Figure 6a), and EPI emits red fluorescence under

DOI: 10.1021/acsami.5b02095
ACS Appl. Mater. Interfaces 2015, 7, 11423−11435

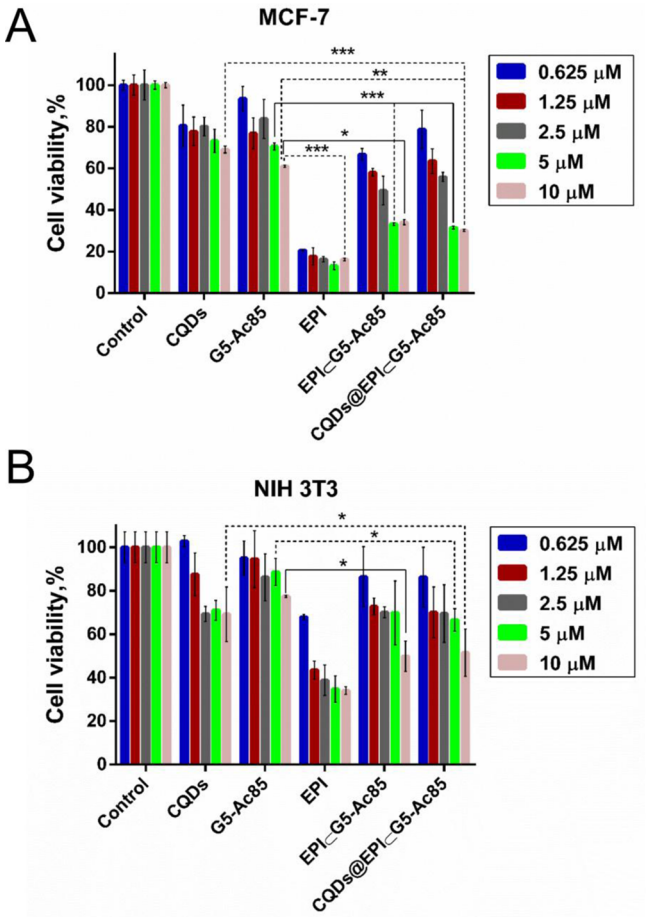

Figure 5. Viability of MCF-7 and NIH 3T3 cells calculated by MTT assay after 48 h of treatment with CQDs, G5-Ac85 dendrimers, EPI, EPI⊂G5-Ac85 complexes, and CQDs@EPI⊂G5-Ac85 hybrids with varying EPI concentrations (0.625, 1.25, 2.5, 5, and 10 μM). EPI⊂G5-Ac85 complexes, CQDs@EPI⊂G5-Ac85 hybrids, and free EPI had equivalent EPI concentrations. CQDs, G5-Ac85, and CQDs@EPI⊂G5-Ac85 hybrids had equivalent weight concentrations. Experiments were performed in triplicate. Two-way ANOVA with Tukey's multiple comparisons test was used to determine statistical difference between the group means (*p < 0.05, **p < 0.005, ***p < 0.001).

green light (Figure 6g). Hoechst 33342 dye was used as a fluorescence marker for the nucleus and emitted blue fluorescence under UV light. After 12 h of incubation, CQDs were mostly internalized in the cell cytoplasm but could not enter the nucleus (Figure 6d). This suggests the cytoplasmic region as the main cellular target of free CQDs.[40,42,46] Interestingly, there was a marked difference in the trafficking of free and encapsulated EPI. Free EPI molecules were mostly localized in the nuclear region as evident from the merged fluorescence image (Figure 6f–h). Probably, free EPI molecules penetrated through the plasma and nuclear membranes to enter the nuclei.[53] Conversely, EPI⊂G5-Ac85 complexes were primarily found distributed in the cytoplasmic region (Figure 6j–l). Moreover, CQDs@EPI⊂G5-Ac85 hybrids were also traced in cell cytoplasm surrounding the nucleus and exhibited colocalization of green and red fluorescence (due to release of both CQDs and EPI, respectively; Figure 6m–p). The location of CQDs@G5-Ac85 hybrids in MCF-7 cells after internalization was visualized using lysotracker red, for fluorescence imaging of lysosomes. MCF-7 cells were incubated with CQDs@G5-Ac85 hybrids for 3 h and were then stained with lysotracker red. After incubation, green fluorescence of hybrids was clearly evident within cells which coincided with the lysotracker red fluorescence (Figure S5). This observation indicated that CQDs@G5-Ac85 hybrids sufficiently accumulated in the cells after internalization and were thereafter transported to lysosomes. These findings suggest lysosomes as the target organelles of CQDs@G5-Ac85 hybrids. The obtained findings demonstrate the significance of luminescent CQDs as fluorescent tracers for cellular delivery of therapeutic agents. Surprisingly, from the fluorescent micrographs, an enhancement in the intensity of the green fluorescent signal of CQDs in CQDs@G5-Ac85 hybrids was monitored. This can be ascribed to the improved delivery and therefore enhanced uptake of CQDs bound to G5-Ac85 dendrimers.

Further, experiments were conducted to quantitate the intracellular uptake of hybrids. For this, MCF-7 cells were incubated with free CQDs, EPI⊂G5-Ac85 complexes, and CQDs@EPI⊂G5-Ac85 hybrids (with an equivalent concentration of CQDs) for 3 h, under the same conditions. After incubation, cells were analyzed using flow cytometry without the use of any other dye. The cellular uptake was measured in terms of percentage of cells expressing green fluorescence (due to uptake of CQDs). The flow cytometric analysis revealed that CQDs were internalized by almost 70% cells compared to cells incubated without CQDs (control). However, about 80% cells could uptake CQDs@EPI⊂G5-Ac85 hybrids under the same parameters (Figure 7A). For EPI⊂G5-Ac85 treated cells, the observed fluorescence (~17%) can primarily be due to the autoflourescent signal of EPI. In a nutshell, both qualitative and quantitative results indicated that G5-Ac85 dendrimers could augment the intracellular distribution and uptake of CQDs. This aspect offers a new horizon in the development of dendrimer based multifunctional vehicles for delivery of imaging and anticancer agents. Although, the exact mechanism of cellular uptake and ultimate cellular fate of nanomaterials in cancer cells is still under investigation. Recent reports suggest clathrin dependent receptor-mediated endocytosis (CME) as the main pathway for internalization of positively charged nanoparticles in MCF-7 cells.[54−56] For CQDs@EPI⊂G5-Ac85 hybrids carrying an overall positive charge, the probable mechanism of internalization could be classical clathrin-mediated endocytosis.

EPI is known to inhibit the topoisomerase II activity in MCF-7 cells with induction of oxidative DNA damage. Thereafter, cells with failed DNA repair mechanisms, undergo apoptosis.[57−59] Subsequently, we examined the effect of EPI on the cell cycle and hence DNA damage by PI staining using a flow cytometer. Figure 7B represents the cell cycle distribution pattern of MCF-7 cells incubated with CQDs, EPI⊂G5-Ac85 complexes, and CQDs@EPI⊂G5-Ac85 hybrids (EPI concentration = 5 μM) for 48 h. The flow cytometric analysis showed that untreated and CQDs treated cells were arrested primarily in the G0/G1 phase. Contrarily, EPI⊂G5-Ac85 complexes or CQDs@EPI⊂G5-Ac85 hybrid treated cells mainly accumulated in the sub G0/G1 phase, i.e., 65.9 ± 1.41% and 75.7 ± 0.85%, respectively, with respect to untreated cells (17 ± 0.42%). Moreover, a reduction in the S phase was monitored upon EPI exposure. This implicates DNA damage by EPI⊂G5-Ac85 and CQDs@EPI⊂G5-Ac85 treatment. A substantial increase in the sub G0/G1 phase and reduction in the S phase population is indicative of an apoptotic mode of cell death.[60,61] After PI staining, CQDs@EPI⊂G5-Ac85 treated cells were examined under FE-SEM to monitor cell morphology alterations. Figure

DOI: 10.1021/acsami.5b02095
ACS Appl. Mater. Interfaces 2015, 7, 11423−11435

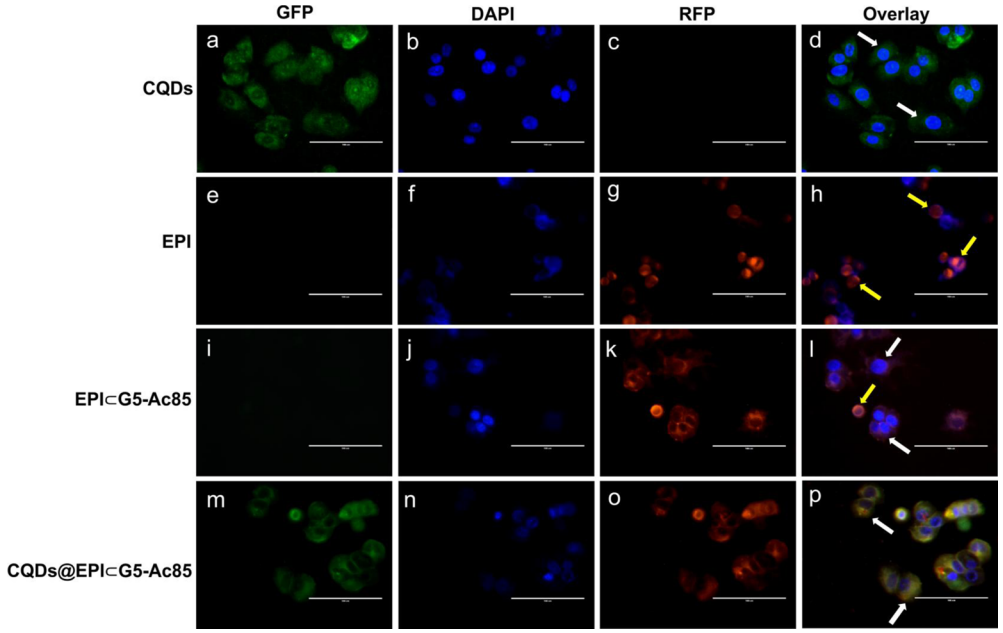

Figure 6. Fluorescence microscope images of MCF-7 cells incubated with free CQDs, free EPI, EPI⊂G5-Ac85 complexes, and CQDs@EPI⊂G5-Ac85 hybrids (with equivalent EPI concentration 5 μM) after 12 h. Intracellular distribution of CQDs is shown in a–d; e–h represent cells treated with EPI; i–l and m–p depicts cells treated with EPI⊂G5-Ac85 and CQDs@EPI⊂G5-Ac85 hybrids, respectively. Yellow arrows, nuclear localization; white arrows, cytoplasmic localization (scale bar = 100 μm).

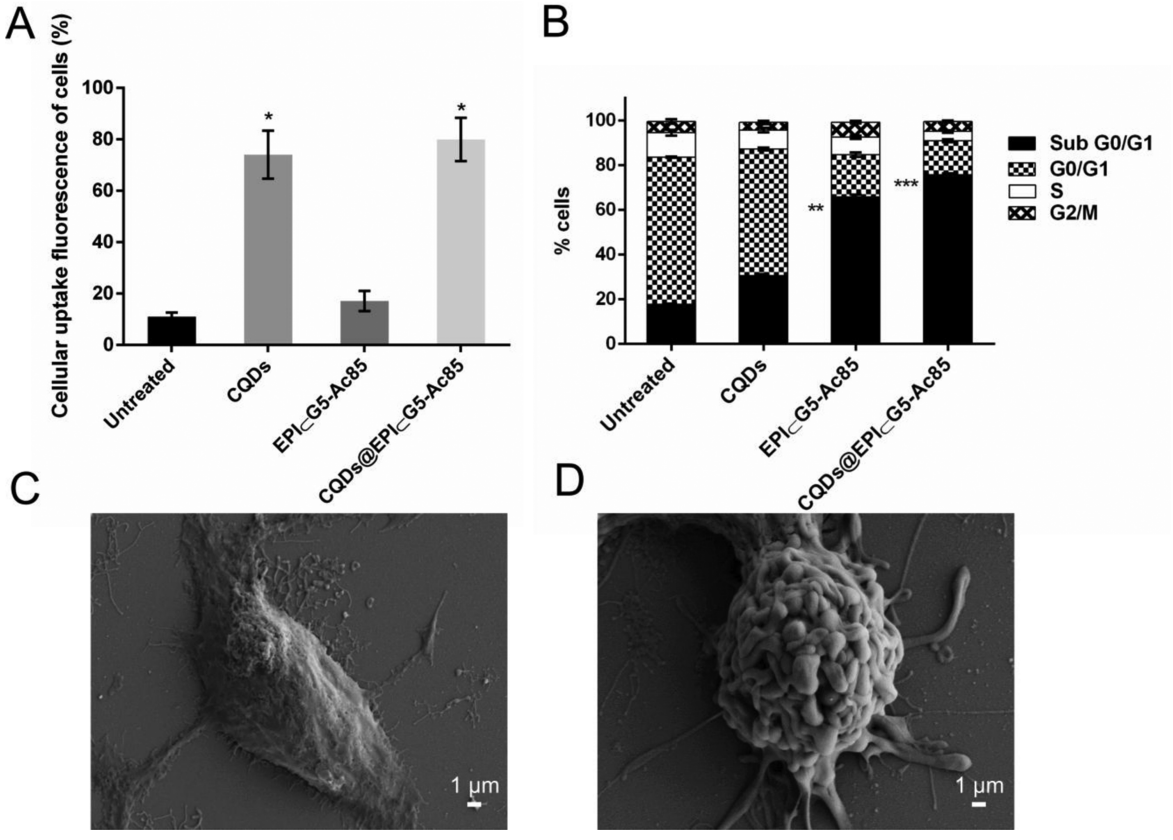

Figure 7. (A) Quantitative cellular uptake in MCF-7 cells after 3 h by flow cytometer. The fluorescence intensity was recorded in channel 02 (505–560 nm). (B) Cell cycle distribution of different samples by flow cytometry. FE-SEM micrographs of (C) untreated and (D) CQDs@EPI⊂G5-Ac85 hybrids treated MCF-7 cell indicating apoptotic cell death (scale bar = 1 μm). Statistical significance is denoted by *$p < 0.05$, **$p < 0.005$, and ***$p < 0.001$.

7C shows the typical morphology of healthy MCF-7 cells. The cells were well adhered to the surface with no signs of membrane constrictions or damage. However, CQDs@EPI⊂G5-Ac85 treated cells were round and loosely attached

DOI: 10.1021/acsami.5b02095
ACS Appl. Mater. Interfaces 2015, 7, 11423–11435

(Figure 7D). Membrane blebbing and the appearance of apoptotic bodies in treated cells confirm the occurrence of apoptosis.[62]

Manifestation of free radical generation can result in oxidative stress in cancer cells, causing apoptosis and finally cell death. The ability of free EPI to induce ROS production in breast cancer cells is well documented.[59] As a proof of concept, we exposed MCF-7 cells to CQDs@EPI⊂G5-Ac85 hybrids with different EPI concentrations for ROS production. The percentage of cells expressing ROS was measured by DCF fluorescence. Figure 8 shows the flow cytometric images of cells with green DCF fluorescence. Each spot in the image reflects the cell expressing ROS. CQDs@EPI⊂G5-Ac85 hybrids were found to induce ROS production in a dose-dependent manner (Figure 8b–e). For instance, CQDs@EPI⊂G5-Ac85 hybrids with 5 μM EPI could elevate the ROS levels by ~86.7% (Figure 8e) with regard to untreated cells (0.61%) (Figure 8a). Such increased cellular oxidative stress can be held responsible for causing DNA damage in cancer cells. It is imperative to mention that fluorescence of CQDs did not interfere during flow measurements owing to its relatively weak signal relative to commercial DCFH-DA dye. Furthermore, we used NIH 3T3 cells to examine the ROS levels in normal cells when exposed to CQDs@EPI⊂G5-Ac85 hybrids. With an increase in the hybrid concentration, the ROS levels in NIH 3T3 cells increased from 5.2% to 13.1%. (Figure S6). However, under similar treatment concentrations, the intracellular ROS production was more in MCF-7 than NIH 3T3 cells. Thus, CQDs@EPI⊂G5-Ac85 hybrids were proficient in inducing apoptosis by causing oxidative stress and, thus, DNA damage in drug resistant breast cancer cells.

To ascertain the molecular signaling pathway involved in CQDs@EPI⊂G5-Ac85 hybrid mediated apoptosis, gene expression analysis was done. Semiquantitative RT-PCR was utilized to validate the expression levels of apoptotic (p53, bax, bad, caspase 3, and c-myc) and antiapoptotic (bcl-xl) genes, respectively. Figure 9A shows the RT-PCR analysis of apoptosis related genes and the computed fold change (Figure 9B). Elevated mRNA expressions of p53, bax, bad, and caspase-3 were observed with down regulation of c-myc and bcl-xl mRNA levels in EPI, EPI⊂G5-Ac85, and CQDs@EPI⊂G5-Ac85 treated samples compared to untreated/CQDs treated cells. The expression of β-actin remained unaltered. A schematic illustration of the apoptotic events involved in CQDs@EPI⊂G5-Ac85 treatment is depicted in Figure 9C.

Internalization of CQDs@EPI⊂G5-Ac85 hybrids causes membrane destabilization and generation of ROS, which in turn triggers the activation of an intrinsic/mitochondrial apoptosis pathway. EPI treatment results in transcriptional activation of the p53 gene, which is pivotal to promoting apoptosis in tumor cells.[63,64] After treatment, the p53 mRNA levels significantly enhanced ($p < 0.005$), which indicates turning-on of p53 mediated gene signaling cascade. Bcl-xl (basal cell lymphoma-extra large), a member of the bcl-2 family of proteins, is known to protect cells from undergoing apoptosis. Hence, suppression of the bcl-xl gene is essential for initiation of apoptotic events.[65] A significant down regulation in the bcl-xl gene ($p < 0.001$) in treated samples marks the onset of apoptosis. The transcription factor p53 further upregulates bax (bcl-2-associated X protein) and bad (bcl-2-associated death promoter) levels, which accelerates apoptosis.[66] Relocalization of bax from the mitochondrial membrane to cytosol leads to outer membrane permeabilization (MOMP) and pore formation to allow cytochrome c (cyt. c) release. The released cyt. c triggers activation of cysteine-aspartic acid proteases (caspase 3) which are the key executioners of apoptosis.[67] Caspase 3 is identified to induce various biochemical changes and morphological changes in cancer cells.[68] In EPI treated cells, a significant upregulation of caspase 3 ($p < 0.005$) corelates with the observed DNA damage and formation of apoptotic bodies. Also, EPI is identified to suppress the c-myc mRNA levels.[69] We also observed

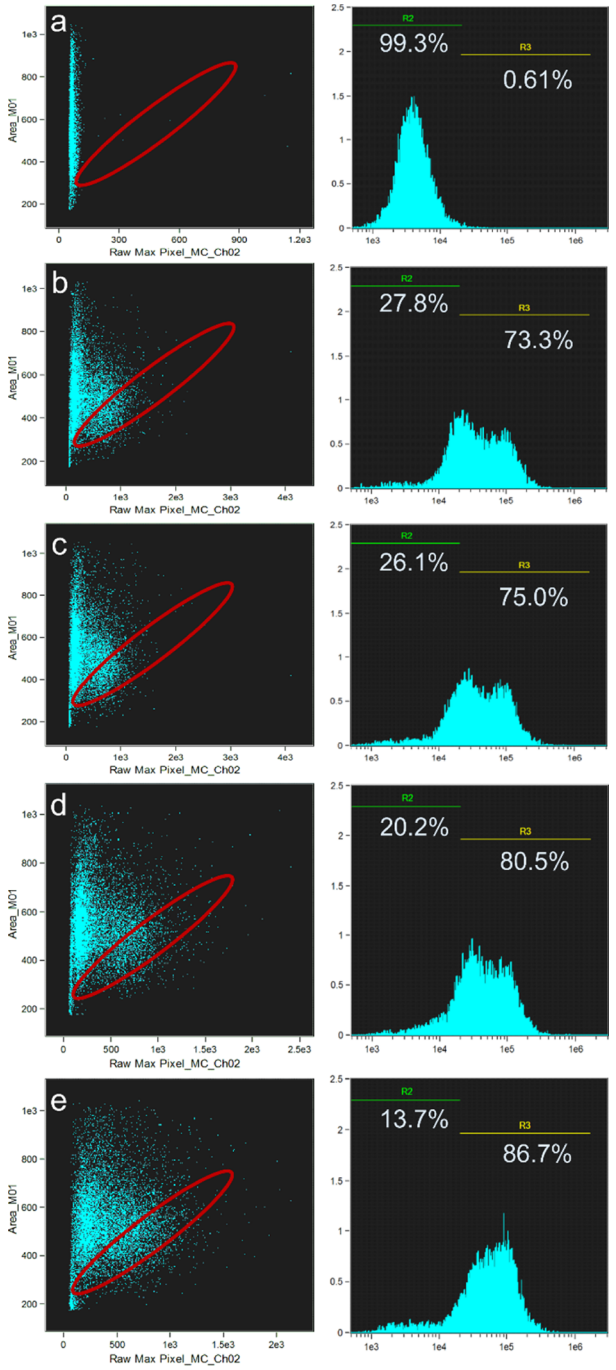

Figure 8. Flow cytometric analysis of ROS production in MCF-7 cells treated with CQDs@EPI⊂G5-Ac85 hybrids with varying concentrations of EPI. Untreated cells are shown in a; b–e depict cells treated with CQDs@EPI⊂G5-Ac85 hybrids with EPI concentrations of 0.625, 1.25, 2.5, and 5 μM, respectively. Left panel: dot plots of DCF fluorescence. Right panel: corresponding fluorescence histogram.

DOI: 10.1021/acsami.5b02095
ACS Appl. Mater. Interfaces 2015, 7, 11423–11435

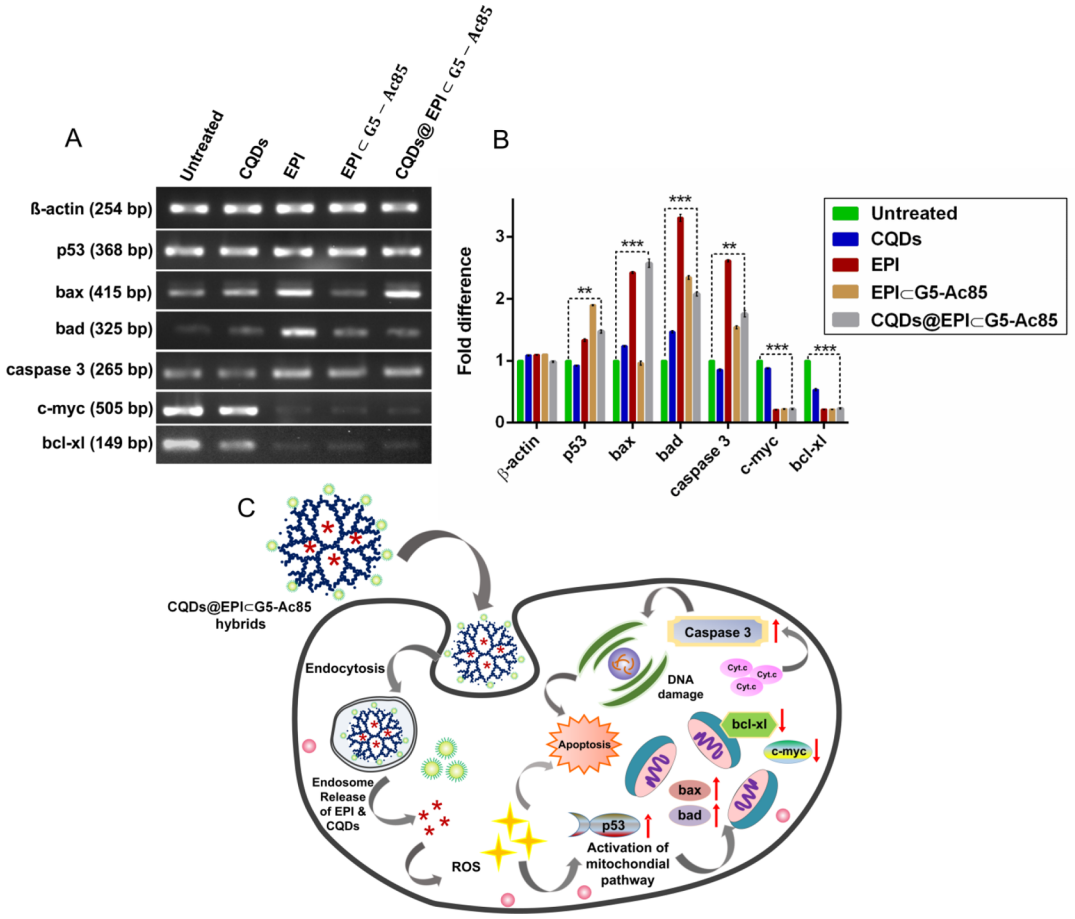

Figure 9. (A) Semiquantitative RT-PCR analysis of apoptotic signaling genes and (B) fold difference in gene expression. Statistical significance between CQDs@EPI⊂G5-Ac85 treated vs untreated MCF-7 cells is denoted by $^{**}p < 0.005$ and $^{***}p < 0.001$. (C) Schematic illustration of cellular uptake and apoptotic events following CQDs@EPI⊂G5-Ac85 hybrid treatment.

drastically reduced c-myc mRNA levels, indicating EPI induced toxicity in breast cancer cells. Altogether, our findings strongly suggest that CQDs@EPI⊂G5-Ac85 hybrids induced apoptosis in breast cancer cells through oxidative DNA damage and trigger p53 mediated gene signaling cascade. Understanding of cellular and molecular mechanisms behind CQDs@EPI⊂G5-Ac85 mediated cell death can be vital in designing strategies for improved cancer therapy. Moreover, such a complicated regulatory pathway necessitates the development of a multifunctional nanovehicle like G5-Ac dendrimers for real-time delivery of epirubicin and fluorescent probes such as CQDs for improved cancer diagnostics and therapy.

4. CONCLUSION

Herein, we report CQDs@EPI⊂G5-Ac85 hybrids for monitoring the cellular distribution of anticancer drug epirubicin (EPI) in MCF-7 cells. Hydroxyl-functionalized CQDs could electrostatically interact with cationic acetylated dendrimers to form fluorescent hybrids. Interestingly, an enhancement in CQDs fluorescence and lifetime was witnessed with CQDs@G5-Ac85 hybrid formation. Moreover, CQDs@G5-Ac85 hybrids can function as a dual-emission system, by combining the green fluorescence of CQDs with the EPI red fluorescence. There steps in the practical utility of CQDs@G5-Ac85 hybrids to track the uptake of chemotherapeutic agents. Further, various cell biological assays confirm the applicability of CQDs@EPI⊂G5-Ac85 hybrids to induce cell death in breast cancer cells. The rationale behind cell killing involves ROS generation to induce DNA fragmentation and triggering of an intrinsic mitochondrial apoptotic pathway. In a nutshell, the present work prompts the applicability of multifunctional CQDs@EPI⊂G5-Ac85 hybrids for cancer imaging and therapy. Further studies on functionalization of CQDs@G5-Ac85 hybrids to attain target specificity are underway.

■ ASSOCIATED CONTENT

Ⓢ Supporting Information

^{1}H NMR spectra, TEM images with size distribution data, lifetime data table, emission spectra, zeta potential results, fluorescence microscopic images, and ROS data are included. The Supporting Information is available free of charge on the ACS Publications website at DOI: 10.1021/acsami.5b02095.

■ AUTHOR INFORMATION

Corresponding Author

*Tel.: 91-1332-285650. Fax: +91-1332-273560. E-mail: pgopifnt@iitr.ernet.in. genegopi@gmail.com.

Notes

The authors declare no competing financial interest.

■ ACKNOWLEDGMENTS

We give sincere thanks to the Science and Engineering Research Board (No. SR/FT/LS-57/2012) and Department of Biotechnology (No. BT/PR6804/GBD/27/486/2012),

DOI: 10.1021/acsami.5b02095
ACS Appl. Mater. Interfaces 2015, 7, 11423−11435

Government of India, for the financial support. I.M. and A.S. are thankful to the Ministry of Human Resource Development, Government of India, for the fellowship. Department of Chemistry and Institute Instrumentation Centre, Indian Institute of Technology Roorkee are sincerely acknowledged for providing various analytical facilities.

REFERENCES

(1) Xie, J.; Lee, S.; Chen, X. Nanoparticle-Based Theranostic Agents. *Adv. Drug Delivery Rev.* **2010**, *62*, 1064−1079.
(2) Janib, S. M.; Moses, A. S.; MacKay, J. A. Imaging and Drug Delivery using Theranostic Nanoparticles. *Adv. Drug Delivery Rev.* **2010**, *62*, 1052−1063.
(3) Wang, Z.; Niu, G.; Chen, X. Polymeric Materials for Theranostic Applications. *Pharm. Res.* **2014**, *31*, 1358−1376.
(4) Wang, D.; Lin, B.; Ai, H. Theranostic Nanoparticles for Cancer and Cardiovascular Applications. *Pharm. Res.* **2014**, *31*, 1390−1406.
(5) Lee, C. C.; MacKay, J. A.; Frechet, J. M. J.; Szoka, F. C. Designing Dendrimers for Biological Applications. *Nat. Biotechnol.* **2005**, *23*, 1517−26.
(6) Stiriba, S. E.; Frey, H.; Haag, R. Dendritic Polymers in Biomedical Applications: From Potential to Clinical Use in Diagnostics and Therapy. *Angew. Chem., Int. Ed.* **2002**, *41*, 1329−1334.
(7) Svenson, S.; Tomalia, D. A. Dendrimers in Biomedical Applications–Reflections on the Field. *Adv. Drug Delivery Rev.* **2005**, *57*, 2106−2129.
(8) Wolinsky, J. B.; Grinstaff, M. W. Therapeutic and Diagnostic Applications of Dendrimers for Cancer Treatment. *Adv. Drug Delivery Rev.* **2008**, *60*, 1037−1055.
(9) Meijer, E. W.; Jansen, J.; Brabander-van den Berg, E. Encapsulation of Guest Molecules into a Dendritic Box. *Science* **1994**, *266*, 1226−1229.
(10) Morgan, M. T.; Carnahan, M. A.; Immoos, C. E.; Ribeiro, A. A.; Finkelstein, S.; Lee, S. J.; Grinstaff, M. W. Dendritic Molecular Capsules for Hydrophobic Compounds. *J. Am. Chem. Soc.* **2003**, *125*, 15485−15489.
(11) Wang, Y.; Guo, R.; Cao, X.; Shen, M.; Shi, X. Encapsulation of 2-Methoxyestradiol within Multifunctional Poly (amidoamine) Dendrimers for Targeted Cancer Therapy. *Biomaterials* **2011**, *32*, 3322−3329.
(12) Zheng, Y.; Fu, F.; Zhang, M.; Shen, M.; Zhu, M.; Shi, X. Multifunctional Dendrimers Modified with Alpha-Tocopheryl Succinate for Targeted Cancer Therapy. *Med. Chem. Commun.* **2014**, *5*, 879−885.
(13) Zhu, J.; Shi, X. Dendrimer-Based Nanodevices for Targeted Drug Delivery Applications. *J. Mater. Chem. B* **2013**, *1*, 4199−4211.
(14) Zhu, J.; Zheng, L.; Wen, S.; Tang, Y.; Shen, M.; Zhang, G.; Shi, X. Targeted Cancer Theranostics Using Alpha Tocopheryl Succinate-Conjugated Multifunctional Dendrimer-Entrapped Gold Nanoparticles. *Biomaterials* **2014**, *35*, 7635−7646.
(15) Tsai, Y. J.; Hu, C. C.; Chu, C. C.; Imae, T. Intrinsically Fluorescent PAMAM Dendrimer as Gene Carrier and Nanoprobe for Nucleic Acids Delivery: Bioimaging and Transfection Study. *Biomacromolecules* **2011**, *12*, 4283−4290.
(16) Kong, L.; Alves, C. S.; Hou, W.; Qiu, J.; Mohwald, H.; Tomas, H.; Shi, X. RGD Peptide-Modified Dendrimer-Entrapped Gold Nanoparticles Enable Highly Efficient and Specific Gene Delivery to Stem Cells. *ACS Appl. Mater. Interfaces* **2015**, *7*, 4833−4843.
(17) Xiao, T.; Hou, W.; Cao, X.; Wen, S.; Shen, M.; Shi, X. Dendrimer-Entrapped Gold Nanoparticles Modified with Folic Acid for Targeted Gene Delivery Applications. *Biomater. Sci.* **2013**, *1*, 1172−1180.
(18) Dufès, C.; Uchegbu, L. F.; Schätzlein, A. G. Dendrimers in Gene Delivery. *Adv. Drug Delivery Rev.* **2005**, *57*, 2177−2202.
(19) Shi, X.; Sun, Kai.; Baker, J. R. Spontaneous Formation of Functionalized Dendrimer-Stabilized Gold Nanoparticles. *J. Phys. Chem. C* **2009**, *112*, 8251−8258.
(20) Matai, I.; Sachdev, A.; Gopinath, P. Multicomponent 5-fluorouracil loaded PAMAM Stabilized-Silver Nanocomposites Synergistically Induce Apoptosis in Human Cancer Cells. *Biomater. Sci.* **2015**, *3*, 457−468.
(21) Naha, P. C.; Davoren, M.; Lyng, F. M.; Byrne, H. J. Reactive Oxygen Species (ROS) Induced Cytokine Production and Cytotoxicity of PAMAM Dendrimers in J774A.1 cells. *Toxicol. Appl. Pharmacol.* **2010**, *246*, 91−99.
(22) Naha, P. C.; Byrne, H. J. Generation of Intracellular Reactive Oxygen Species and Genotoxicity Effect to Exposure of Nanosized Polyamidoamine (PAMAM) Dendrimers in PLHC-1 cells In Vitro. *Aquat. Toxicol.* **2013**, *132*−*133*, 61−72.
(23) Naha, P. C.; Davoren, M.; Casey, A.; Byrne, H. J. An Ecotoxicological Study of Poly(amidoamine) Dendrimers-Toward Quantitative Structure Activity Relationships. *Environ. Sci. Technol.* **2009**, *43*, 6864−6869.
(24) Mukherjee, S. P.; Lyng, F. M.; Garcia, A.; Davoren, M.; Byrne, H. J. Mechanistic Studies of In Vitro Cytotoxicity of Poly(amidoamine) Dendrimers in Mammalian Cells. *Toxicol. Appl. Pharmacol.* **2010**, *248*, 259−268.
(25) Hong, S.; Bielinska, A. U.; Mecke, A.; Keszler, B.; Beals, J. L.; Shi, X.; Balogh, L.; Orr, B. G.; Baker, J. R. Interaction of Poly(amidoamine) Dendrimers with Supported Lipid Bilayers and Cells: Hole Formation and the Relation to Transport. *Bioconjugate Chem.* **2004**, *15*, 774−782.
(26) Mecke, A.; Majoros, I. J.; Patri, A. K.; Baker, J. R., Jr.; Banaszak Holl, M. M.; Orr, B. G. Lipid Bilayer Disruption by Polyamidoamine Dendrimers: The Role of Generation and Capping Group. *Langmuir* **2005**, *21*, 10348−10354.
(27) Lee, H.; Larson, R. G. Lipid Bilayer Curvature and Pore Formation Induced by Charged Linear Polymers and Dendrimers: The Effect of Molecular Shape. *J. Phys. Chem. B* **2008**, *112*, 12279−12285.
(28) Wang, W.; Xiong, W.; Wan, J. L.; Sun, X. H.; Xu, H. B.; Yang, X. L. The Decrease of PAMAM Dendrimer-Induced Cytotoxicity by PEGylation via Attenuation of Oxidative Stress. *Nanotechnology* **2009**, *20*, 105−103.
(29) Liu, H.; Wang, H.; Xu, Y.; Guo, R.; Wen, S.; Huang, Y.; Liu, W.; Shen, M.; Zhao, J.; Zhang, G.; Shi, X. Lactobionic Acid-Modified Dendrimer-Entrapped Gold Nanoparticles for Targeted Computed Tomography Imaging of Human Hepatocellular Carcinoma. *ACS Appl. Mater. Interfaces* **2014**, *6*, 6944−6953.
(30) Liu, H.; Wang, H.; Xu, Y.; Shen, M.; Zhao, J.; Zhang, G.; Shi, X. Synthesis of PEGylated Low Generation Dendrimer-Entrapped Gold Nanoparticles for CT Imaging Applications. *Nanoscale* **2014**, *6*, 4521−4526.
(31) Majoros, I. J.; Keszler, B.; Woehler, S.; Bull, T.; Baker, J. R. Acetylation of Poly(amidoamine) Dendrimers. *Macromolecules* **2003**, *36*, 5526−5529.
(32) Hu, J.; Su, Y.; Zhang, H.; Xu, T.; Cheng, Y. Design of Interior-Functionalized Fully Acetylated Dendrimers for Anticancer Drug Delivery. *Biomaterials* **2011**, *32*, 9950−9959.
(33) Minotti, G.; Menna, P.; Salvatorelli, E.; Cairo, G.; Gianni, L. Anthracyclines: Molecular Advances and Pharmacologic Developments in Antitumor Activity and Cardiotoxicity. *Pharmacol. Rev.* **2004**, *56*, 185−229.
(34) Torti, F. M.; Bristow, M. M.; Lum, B. L.; Carter, S. K.; Howes, A. E.; Aston, D. A.; Brown, B. W., Jr.; Hannigan, J. F., Jr.; Meyers, F. J.; Mitchell, E. P.; Billingham, M. E. Cardiotoxicity of Epirubicin and Doxorubicin: Assessment by Endomyocardial Biopsy. *Cancer Res.* **1986**, *46*, 3722−3727.
(35) Xu, X. Y.; Ray, R.; Gu, Y. L.; Ploehn, H. J.; Gearheart, L.; Raker, K.; Scrivens, W. A. Electrophoretic Analysis and Purification of Fluorescent Single-Walled Carbon Nanotube Fragments. *J. Am. Chem. Soc.* **2004**, *126*, 12736−12737.
(36) Sun, Y. P.; Zhou, B.; Lin, Y.; Wang, W.; Fernando, K. A. S.; Pathak, P.; Meziani, M. J.; Harruff, B. A.; Wang, X.; Wang, H.; Luo, P. G.; Yang, H.; Kose, M. E.; Chen, B.; Veca, L. M.; Xie, S. Y. Quantum

DOI: 10.1021/acsami.5b02095
ACS Appl. Mater. Interfaces 2015, 7, 11423−11435

Sized Carbon Dots for Bright and Colorful Photoluminescence. *J. Am. Chem. Soc.* **2006**, *128*, 7756−7757.
(37) Ma, Z.; Zhang, Y. L.; Wang, L.; Ming, H.; Li, H. T.; Zhang, X.; Wang, F.; Liu, Y.; Kang, Z. H.; Lee, S. T. Bioinspired Photoelectric Conversion System Based on Carbon Quantum Dot Doped Dye−Semiconductor Complex. *ACS Appl. Mater. Interfaces* **2013**, *5*, 5080−5084.
(38) Sachdev, A.; Matai, I.; Kumar, S. U.; Bhushan, B.; Dubey, P.; Gopinath, P. A Novel One-Step Synthesis of PEG Passivated Multicolour Fluorescent Carbon Dots for Potential Biolabeling Application. *RSC Adv.* **2013**, *3*, 16958−16961.
(39) Sachdev, A.; Matai, I.; Gopinath, P. Implications of Surface Passivation on Physicochemical and Bioimaging Properties of Carbon Dots. *RSC Adv.* **2014**, *4*, 20915−20921.
(40) Sachdev, A.; Matai, I.; Gopinath, P. Dual-Functional Carbon Dots−Silver@Zinc Oxide Nanocomposite: In Vitro Evaluation of Cellular Uptake and Induction of Apoptosis. *J. Mater. Chem. B* **2015**, *3*, 1217−1229.
(41) Datta, K. K. R.; Kozak, O.; Ranc, V.; Havrdová, M.; Bourlinos, A. B.; Šafářová, K.; Holá, K.; Tománková, K.; Zoppellaro, G.; Otyepkaa, M.; Zbořil, R. Quaternized Carbon Dot-Modified Graphene Oxide for Selective Cell Labelling − Controlled Nucleus and Cytoplasm Imaging. *Chem. Commun.* **2014**, *50*, 10782−10785.
(42) Zhou, L.; Li, Z.; Liu, Z.; Ren, J.; Qu, X. Luminescent Carbon Dot-Gated Nanovehicles for pH-Triggered Intracellular Controlled Release and Imaging. *Langmuir* **2013**, *29*, 6396−6403.
(43) Zong, J.; Yang, X.; Trinchi, A.; Hardin, S.; Cole, I.; Zhu, Y.; Li, C.; Muster, T.; Wei, G. Photoluminescence Enhancement of Carbon Dots by Gold Nanoparticles Conjugated via PAMAM dendrimers. *Nanoscale* **2013**, *5*, 11200−11206.
(44) Dong, W.; Zhou, S.; Dong, Y.; Wang, J.; Ge, X.; Sui, L. The Preparation of Ethylenediamine-Modified Fluorescent Carbon Dots and their use in Imaging of Cells. *Luminescence* **2015**, DOI: 10.1002/bio.2834.
(45) Liu, C.; Zhang, P.; Zhai, X.; Tian, F.; Li, W.; Yang, J.; Liu, Y.; Wang, H.; Wang, W.; Liu, W. Nano-carrier for Gene Delivery and Bioimaging based on Carbon Dots with PEI-Passivation Enhanced Fluorescence. *Biomaterials* **2012**, *33*, 3604−3613.
(46) Wang, Q.; Huang, X.; Long, Y.; Wang, X.; Zhang, H.; Zhu, R.; Liang, L.; Teng, P.; Zheng, H. Hollow Luminescent Carbon Dots for Drug Delivery. *Carbon* **2013**, *59*, 192−199.
(47) Majoros, I. J.; Myc, A.; Thomas, T.; Mehta, C. B.; Baker, J. R., Jr. PAMAM Dendrimer-based Multifunctional Conjugate for Cancer Therapy: Synthesis, Characterization, and Functionality. *Biomacromolecules* **2006**, *7*, 572−579.
(48) Li, X.; Gao, C.; Wu, Y.; Cheng, C. Y.; Xiac, W.; Zhang, Z. Combination Delivery of Adjudin and Doxorubicin via Integrating Drug Conjugation and Nanocarrier Approaches for the Treatment of Drug-resistant Cancer Cells. *J. Mater. Chem. B* **2015**, *3*, 1556−1564.
(49) Huang, R.; Ke, W.; Liu, Y.; Jiang, C.; Pei, Y. The Use of Lactoferrin as a Ligand for Targeting the Polyamidoamine-based Gene Delivery System to the Brain. *Biomaterials* **2008**, *29*, 238−246.
(50) Tong, G.; Wang, J.; Wang, R.; Guo, X.; He, L.; Qiu, F.; Wang, Ge.; Zhu, B.; Zhu, X.; Liu, T. Amorphous Carbon Dots with High two-photon Fluorescence for Cellular Imaging Passivated by Hyperbranched Poly(amino amine). *J. Mater. Chem. B* **2015**, *3*, 700−706.
(51) Maiti, P. K.; Cagin, T.; Lin, S. T.; Goddard, W. A. Effect of Solvent and pH on the Structure of PAMAM Dendrimers. *Macromolecules* **2005**, *38*, 979−991.
(52) Dong, Y.; Wang, R.; Li, H.; Shao, J.; Chi, Y.; Lin, X.; Chen, G. Polyamine-Functionalized Carbon Quantum Dots for Chemical Sensing. *Carbon* **2012**, *50*, 2810−2815.
(53) Yordanov, G.; Evangelatov, A.; Skrobanska, R. Epirubicin Loaded to Pre-Polymerized Poly(butyl cyanoacrylate) Nanoparticles: Preparation and In Vitro Evaluation in Human Lung Adenocarcinoma Cells. *Colloids Surf., B* **2013**, *107*, 115−123.
(54) Sahay, G.; Alakhova, D. Y.; Kabanov, A. V. Endocytosis of Nanomedicines. *J. Controlled Release* **2010**, *145*, 182−195.
(55) Kitchens, K. M.; Foraker, A. B.; Kolhatkar, R. B.; Swaan, P. W.; Ghandehari, H. Endocytosis and Interaction of Poly (amidoamine) Dendrimers with Caco-2 cells. *Pharm. Res.* **2007**, *24*, 2138−2145.
(56) Kitchens, K. M.; Kolhatkar, R. B.; Swaan, P. W.; Ghandehari, H. Endocytosis Inhibitors prevent Poly(amidoamine) Dendrimer Internalization and Permeability across Caco-2 cells. *Mol. Pharmaceutics.* **2008**, *5*, 364−369.
(57) Fornari, F. A.; Randolph, J. K.; Yalowich, J. C.; Ritke, M. K.; Gewirtz, D. A. Interference by Doxorubicin with DNA Unwinding in MCF-7 Breast Tumor Cells. *Mol. Pharmacol.* **1994**, *45*, 649−656.
(58) Olinski, R.; Gackowski, D.; Foksinski, M.; Rozalski, R.; Roszkowski, K.; Jaruga, P. Oxidative DNA damage: Assessment of the Role in Carcinogenesis, Atherosclerosis, and Acquired Immunodeficiency Syndrome. *Free Radical Biol. Med.* **2002**, *33*, 192−200.
(59) Lo, Y. L.; Wang, W. Formononetin Potentiates Epirubicin-Induced Apoptosis via ROS Production in HeLa cells In Vitro. *Chem. Biol. Interact.* **2013**, *205*, 188−197.
(60) Riccardi, C.; Nicoletti, I. Analysis of Apoptosis by Propidium Iodide Staining and Flow Cytometry. *Nat. Protoc.* **2006**, *1*, 1458−1461.
(61) Darzynkiewicz, Z.; Bruno, S.; Del, B. G.; Gorczyca, W.; Hotz, M. A.; Lassota, P.; Traganos, F. Features of Apoptotic cells Measured by Flow Cytometry. *Cytometry* **1992**, *13*, 795−808.
(62) Rello, S.; Stockert, J. C.; Moreno, V.; Gámez, A.; Pacheco, M.; Juarranz, A.; Cañete, M.; Villanueva, A. Morphological Criteria to Distinguish Cell Death Induced by Apoptotic and Necrotic Treatments. *Apoptosis* **2005**, *10*, 201−208.
(63) Hu, D. G.; Rogers, A.; Mackenzie, P. I. Epirubicin Upregulates UDP glucuronosyltransferase 2B7 Expression in Liver Cancer cells via the p53 pathway. *Mol. Pharmacol.* **2014**, *85*, 887−897.
(64) Millour, J.; de Olano, N.; Horimoto, Y.; Monteiro, L. J.; Langer, J. K.; Aligue, R.; Hajji, N.; Lam, E. W. ATM and p53 Regulate FOXM1 Expression via E2F in Breast Cancer Epirubicin Treatment and Resistance. *Mol. Cancer Ther.* **2011**, *10*, 1046−1058.
(65) Chao, D. T.; Korsmeyer, S. J. BCL-2 family: Regulators of Cell Death. *Annu. Rev. Immunol.* **1998**, *16*, 395−419.
(66) Wolter, K. G.; Hsu, Y. T.; Smith, C. L.; Nechushtan, A.; Xi, X. G.; Youle, R. J. Movement of Bax from the Cytosol to Mitochondria During Apoptosis. *J. Cell Biol.* **1997**, *139*, 1281−1292.
(67) Liu, X.; Kim, C. N.; Yang, J.; Jemmerson, R.; Wang, X. Induction of Apoptotic Program in Cell-Free Extracts: Requirement for dATP and cytochrome c. *Cell* **1996**, *86*, 147−157.
(68) Porter, A. G.; Jänicke, R. U. Emerging Roles of Caspase-3 in Apoptosis. *Cell Death Differ.* **1999**, *6*, 99−104.
(69) Lee, Y. K.; Lin, T. H.; Chang, C. F.; Lo, Y. L. Galectin-3 Silencing Inhibits Epirubicin-Induced ATP Binding Cassette Transporters and Activates the Mitochondrial Apoptosis Pathway via *β*-catenin/GSK-3*β* Modulation in Colorectal Carcinoma. *PLoS One* **2013**, *8*, 82478.

DOI: 10.1021/acsami.5b02095
ACS Appl. Mater. Interfaces 2015, 7, 11423−11435